2021-01-0411 Published 06 Apr 2021

Cold Flow Simulation of a Dual-Fuel Engine for Diesel-Natural Gas and Diesel-Methanol Fuelling Conditions

Gilles Decan and Bert De Buyzerie Ghent University

Tommaso Lucchini and Gianluca D'Errico Politecnico di Milano

Sebastian Verhelst Ghent University

Citation: Decan, G., De Buyzerie, B., Lucchini, T., D'Errico, G. et al., "Cold Flow Simulation of a Dual-Fuel Engine for Diesel-Natural Gas and Diesel-Methanol Fuelling Conditions," SAE Technical Paper 2021-01-0411, 2021, doi:10.4271/2021-01-0411.

Abstract

In this work, the possibility to perform a cold-flow simulation as a way to improve the accuracy of the starting conditions for a combustion simulation is examined. Specifically, a dual-fuel marine engine running on methanol/diesel and natural gas/diesel fueling conditions is investigated. Dual-fuel engines can provide a short-term solution to cope with the more stringent emission legislations in the maritime sector. Both natural gas and methanol appear to be interesting alternative fuels that can be used as main fuel in these dual-fuel engines. Nevertheless, it is observed that combustion problems occur at part load using these alternative fuels. Therefore, different methods to increase the combustion efficiency at part load are investigated. Numerical simulations prove to be very suitable hereto, as they are an efficient way to study the effect of different parameters on the combustion characteristics. These simulations often describe the engine with a limited engine geometry neglecting the inlet and exhaust duct. This gives rise to the need to assume certain starting conditions such as the turbulence coming from the intake valve and the homogeneity of the air/fuel mixture entering the combustion chamber. Hence this work presents the execution of a cold-flow simulation taking into account the whole engine geometry that can provide more realistic initialization values for combustion simulations.

Introduction

The past decade has been marked by some fundamental changes in the emission legislation of the marine sector. A reduction of CO2 emissions of 40% by 2030 compared to 1990 was imposed by the European Union (EU) following the Paris climate conference in 2015 [1]. Additionally, a reduction of harmful exhaust gas emissions such as NO_X -, SO_X - and PM emissions was introduced by the International Maritime Organization (IMO) in 2011 when the Tier II amendment entered into force. Later, in 2016, the Tier III amendment took effect, resulting in even more stringent pollution emission limits [2].

In the maritime sector, the use of robust diesel engines is the most favored propulsion method. To meet the new emission legislations, these have to be equipped with expensive after-treatment systems such as selective catalytic reduction (SCR), diesel particulate filters (DPF) and exhaust gas recirculation (EGR) systems [3]. Therefore, to be able to meet the more stringent emission legislations in a more economically viable way, alternative propulsion methods are introduced.

A cost-effective way to decrease emissions while maintaining the high power output and robustness of a diesel engine is to retrofit the already installed marine diesel engines to dual-fuel operation [4]. A secondary fuel is injected or inducted in the inlet manifold to form a premixed air-fuel mixture which is ignited in the combustion chamber using the auto-ignition of a small pilot diesel spray at top dead center (TDC) [5]. By making an intelligent choice of the secondary fuel, emissions can be reduced drastically while maintaining a comparable power output.

Natural gas (NG) as an alternative fuel has some attractive properties. It is available in several areas worldwide at encouraging prices and can be produced from an abundant selection of resources. It is also characterized by the lowest carbon-to-hydrogen ratio of all fossil fuels and will thus by its chemical composition result in lower CO2 emissions. Additionally, as NG has no C-C bonds in its chemical structure, its combustion will not result in the formation of soot. Nevertheless, NG consists of 87 - 96 % methane, which has a global warming potential that is 25 times greater than CO2. Extensive care would thus have to be taken to avoid the leakage of NG [7].

The use of NG as secondary fuel in dual-fuel engines has already been described extensively. Experimental results from Imran et al. [8] show a comparison between the engine characteristics in normal diesel and dual-fuel NG/diesel operation. It appeared that no significant difference was observed in

thermal efficiency between the normal and dual-fuel operation. However, a small reduction of the thermal efficiency in dual-fuel condition was observed at lower power. This was attributed to the failure of the pilot fuel to ignite and sustain an adequate combustion of the lean natural gas-air mixture. The higher specific heat capacity of natural gas resulted in an overall reduced in-cylinder temperature. As the formation of NO_x is highly dependent on the in-cylinder temperature, a reduced temperature will result in a reduced NO_x formation. A reduction in NO_x-emissions of up to 53% at low power was observed. However, at the highest power, a small increase in NO_x-emissions was observed due to the higher in-cylinder temperatures. Due to the lower carbon-to-hydrogen ratio, a decrease in CO2-emissions of 23-30% was observed over the whole power spectrum. Nevertheless, at low power conditions, the lean NG-air mixture causes inefficient flame propagation resulting in an increase of hydrocarbon (HC) emissions of up to 800%.

It thus becomes clear that especially at low and part load, combustion problems occur in the NG dual-fuel operation. These result in a decrease in thermal efficiency and increase in HC emissions. This increase in HC emissions implies that a substantial amount of NG is not burned and is emitted. This results in the release of methane into the atmosphere. Therefore, research is being executed to increase the combustion efficiency at part load and improve the overall NG dual-fuel operation.

Different methods to increase the combustion efficiency are examined such as modifying the pilot diesel injection [4, 9] or utilizing hot EGR [10]. This research often involves the use of numerical combustion simulations as a fast and efficient way to verify the influence of different parameters on the combustion efficiency. However, many of these simulations only consider the geometry of the combustion chamber to perform the combustion simulations, neglecting the influence of the geometry of the intake and exhaust duct [4, 9, 10]. Therefore, effects such as turbulence and flow motion coming from the intake duct and improper scavenging resulting in internal EGR are not considered whereas they could have an influence on the combustion process.

Consequently, the magnitude of these effects will be studied in this work by performing a 3D cold-flow simulation taking into account the geometry of the combustion chamber, inlet and exhaust. This way, a quantification can be made of the simplifications that are done in a combustion simulation. The results of the cold-flow simulation can subsequently be used to initialize a combustion simulation to simulate a more realistic combustion process.

The use of natural gas as secondary fuel in a dual-fuel engine gives rise to problems with combustion efficiency resulting in high HC emissions and a lower thermal efficiency. Additionally, methane slip could occur, being a much more harmful greenhouse gas than CO_2 and therefore definitely to be avoided. Therefore, it is also worthwhile to look into other alternative fuels. Methanol promises to be a good alternative. Methanol is a liquid fuel that can be produced from an abundant number of possible feedstocks such as NG, coal, biomass and CO_2 [11]. Therefore, it could be possible to produce "renewable" methanol in the future. Furthermore, it has some attractive physical properties for the use in dual-fuel combustion strategies.

Table 1 shows a comparison between the physical properties of methanol and NG. Methanol has a higher heating value of stoichiometric mixture, resulting in a possible reduction in fuel consumption. Similar to NG, no C-C bonds are present in methanol, resulting in no soot being formed due to the combustion of methanol. Additionally, methanol exhibits a higher laminar burning velocity and an additional oxygen atom in its chemical structure (CH3OH). This could make it possible to maintain a higher combustion efficiency, even at low load. Furthermore, a reduction in NO_x-emissions is also expected as methanol has a high latent heat of vaporization which reduces the ambient temperature upon evaporation. Finally, the lower carbon content of methanol will result in even lower CO_2-emissions [12].

The physical properties of methanol such as the higher laminar flame speed and additional oxygen atom would generally result in an improved combustion efficiency. Nevertheless, it is observed that at part load the methanol-air mixture can become too lean in certain areas causing stable combustion to be compromised [13]. Therefore, the substitution ratio is limited at low loads to prevent misfire and/or incomplete combustion when too much methanol is introduced. At high load, the substitution ratio is also limited as knocking can occur due to the high degree of premixed combustion and the high compression ratio of a diesel engine. This generally leads to reported diesel substitution ratios (DSR) between 17% and 67% [14]. The DSR is the ratio of eliminated diesel mass flow in dual-fuel operation to the diesel mass flow in conventional diesel operation.

Compared to conventional diesel operation, the use of methanol in dual-fuel operation does generally not affect the maximum engine load. Nevertheless, Coulier et al. [15] state that no general conclusion can be drawn about the engine efficiency as sometimes a drop in efficiency occurs at the full load range. Additionally, due to the unstable combustion that can occur at low loads, an increase in the coefficient of variability (COV) can be observed. Concerning emission characteristics, the use of methanol in dual-fuel operation results in a decrease of NO_x-emissions in both low and high loads. Dierickx et al. [3,14] converted a diesel engine to a methanol/diesel dual-fuel engine and reported an average relative decrease in specific NO-emissions of 61%. Additionally, a reduction in PM emissions of 95% was reported due to the higher amount of premixed combustion and the absence of C-C bonds in methanol. It can be seen however that CO- and HC-emissions tend to increase compared to conventional diesel operation due to the unstable combustion at low load.

TABLE 1 Comparison of the physical properties of NG and methanol

Fuel properties	Natural gas	Methanol
LHV (MJ/kg)	48.6	19.7
Stoichiometric AFR	17.2	6.5
Cetane number	<0	3
Octane number	130	109
Auto-ignition temp. (°C)	650	470
Carbon content (%)	75	37.5
Max. LBV (m/s)	0.4	0.5

Since no overall conclusion can be drawn about the engine efficiency in dual-fuel combustion mode, little can be said about CO_2-emissions [15]. But as already stated before, because of the lower carbon content of methanol, a general reduction in CO_2-emissions is expected.

To optimize the methanol dual-fuel operation, different studies are performed using numerical simulations. However, as already mentioned previously, similarly like during natural gas/diesel dual-fuel operation, these simulations often neglect the intake and exhaust geometry. As methanol is injected in the intake manifold, the assumption is often made that a homogeneous methanol-air mixture is present at the intake valves. Nevertheless, in real-life applications, this is almost never the case as turbulence, methanol injection pressure and the injector geometry determine the evaporation and mixing rate of the injected methanol. To have a better understanding of the influence of these factors, a 3D CFD cold flow simulation of the cylinder, inlet and exhaust is performed in this work with emphasis on the mixing, evaporation, and distribution of methanol at the intake manifold. This should provide a better understanding of these phenomena and give valuable data for the initialization of closed cycle simulations. Significant reductions in computation time could thereby be obtained during the analysis of combustion simulations, while maintaining accurate information on in-cylinder composition and flow behavior.

Methodology

The open-source software OpenFOAM is used to perform the cold-flow simulations with the additional LibICE library developed at the polytechnic university of Milan. From this additional library, a custom PIMPLE solver is used which is developed especially to be able to calculate cold-flow ICE simulations. To take into account turbulence, a standard k-ε turbulence model is used.

The CFD method is used to simulate a marine engine during both natural gas/diesel and methanol/diesel operation. The studied engine is a single-cylinder test engine by WTZ Roßlau, representative of an ABC 6-in-line DZ engine. The main engine features and valve timings are reported in Table 2 for both simulations. For both simulations, the simulation will start at the opening of the exhaust valve.

TABLE 2 Properties of the WTZ Roßlau engine for both natural gas and methanol operation.

	Natural gas	Methanol
Stroke (mm)	290	
Bore (mm)	240	
Total displacement (cm³)	13,120	
Compression ratio	12.1	
#valves per cylinder	4	
Intake Valve Opening (IVO)	328 °CA	279 °CA
Intake Valve Closing (IVC)	608 °CA	599 °CA
Exhaust Valve Opening (EVO)	104 °CA	97 °CA
Exhaust Valve Closing (EVC)	382 °CA	434 °CA

FIGURE 1 Engine geometries at BDC for the gas dynamics simulations (left = NG case, right = methanol case with elongated inlet duct).

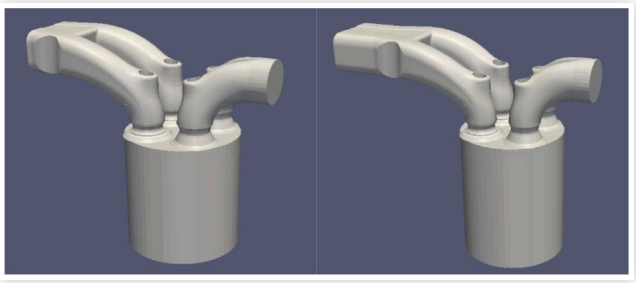

FIGURE 2 Position of the methanol injector in the intake manifold

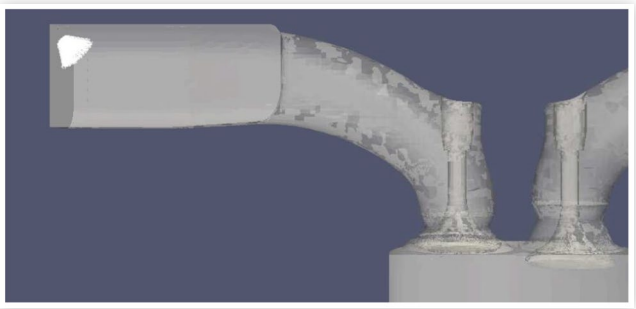

The mesh is designed taking care that a refinement is present at critical locations such as the valve openings, near the wall and at sharp edges in the geometry. For the NG mesh, this results in a grid with approximately 845,000 cells at BDC and 809,000 cells at TDC. For the methanol mesh, approximately 847,000 cells at BDC and 843,000 cells at TDC are used. Figure 1 shows the geometries for both simulations at BDC. In the methanol simulation, the inlet duct is prolonged to be able to inject the methanol spray at the same position as in the test engine.

In the methanol simulation, a methanol spray is injected in the intake manifold. Equally to the experimental setup, two injectors are used that both inject 0.972g methanol over a span of 244 °CA. The start of injection is at 180 °CA. As no experimental mass flow rate profile is known, a uniform injection mass flow rate profile is used. Furthermore, for each injector, the spray is represented by 100,000 parcels. This number was not chosen arbitrary. It was seen that compared with simulations using 500,000 and 1,500,000 parcels, the same results were obtained at a much faster computational speed. In Figure 2, the exact position of the methanol injectors is visualized.

Validation

In this section, the results of both the simulations (NG and methanol) are validated by comparing the simulated pressure traces with the experimental pressure traces. The pressure

trace proves to be a valuable validation tool since the in-cylinder pressure is dependent on a large number of parameters such as trapped mass, in-cylinder temperature and cylinder volume. Therefore, if one of these parameters is modelled incorrectly, the simulated pressure trace will most likely deviate from the experimental in-cylinder pressure trace.

Natural Gas/Diesel Operation

Figure 3 shows a comparison of the simulated and experimental pressure traces at full load and 1000 rpm. It can be seen that a decent overlap is achieved between the two pressure profiles. Around 720 °CA, combustion occurs in the experimental setup, resulting in a sudden pressure increase. Since no combustion is modelled in the cold-flow simulation, this pressure increase is not observed in the simulated pressure trace.

At the end of the exhaust stroke (@360°CA), a small increase in the experimental pressure trace can be observed which is not present in the simulated pressure trace. This small pressure increase in the experimental pressure trace could be due to an effective negative valve overlap present in the test engine. The valve timing measured on the camshaft was provided for the experimental setup and exhibits a small positive valve overlap. However, due to the compliance of the rocker arm and valve stem, the valve timing at the valve itself could be different and an effective small negative valve overlap could be obtained. Since the valve timing at the camshaft is used in the simulation, a positive valve overlap is present. Therefore, no gas can get trapped in the cylinder resulting in no compression and pressure increase.

To validate this hypothesis, a second simulation was performed using an adapted valve timing to exhibit a small negative valve overlap. The pressure trace of this simulation, together with the pressure traces of the previous simulation and experimental setup are depicted in Figure 4. This figure shows a close-up of the pressure traces around 360°CA. Where no pressure increase is observed in the simulation with normal valve timing, a small pressure increase at 360°CA is observed in the simulation with adapted valve timing. Therefore, it can be stated that the pressure increase around 360 °CA, as observed in the experimental pressure trace, is indeed due to a small negative valve overlap. However, since the exact amount of negative valve overlap is difficult to retrieve, and the obtained differences are small, especially during the compression phase, the main zone of interest, the NG simulation is performed using the initial valve timings obtained at the camshaft.

To verify if the validity of the model can also be extended to different engine loading conditions, the model is also validated against a different experimental test at 75% load and 1000 rpm. As can be seen from Figure 5, once again a good overlap is obtained and the same observation can be made as in the simulation at 100% load about the small pressure peak in the experimental pressure at 360 °CA.

The model thus successfully represents the real engine processes that occur in the experimental engine in different loading conditions.

FIGURE 3 Comparison simulated and experimental pressure traces at 100% load.

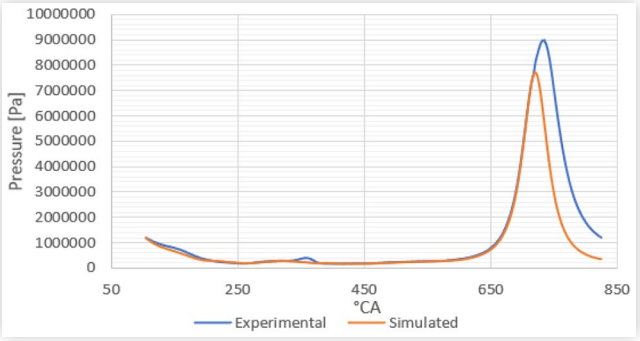

FIGURE 4 Comparison pressure trace at 360 °CA with adapted valve timing.

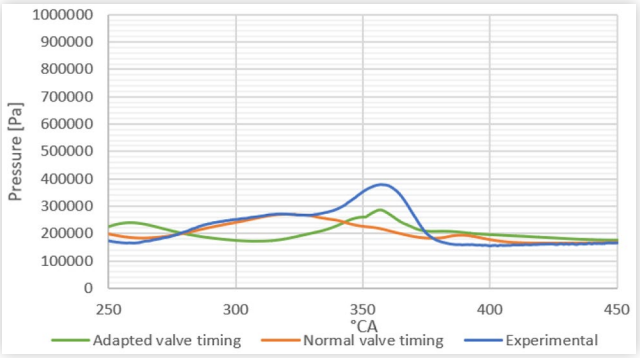

FIGURE 5 Comparison simulated and experimental pressure traces at 75% load.

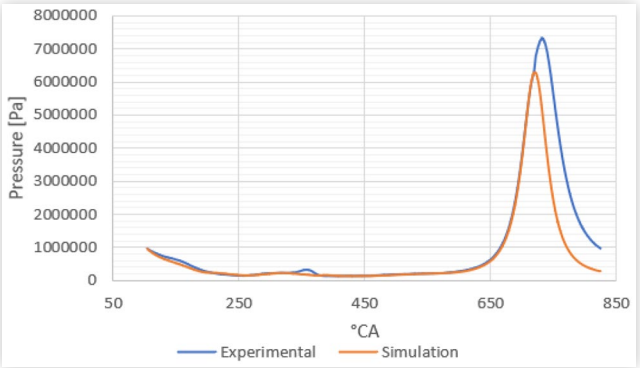

Methanol/Diesel Operation

To examine the methanol cold-flow simulation, two simulations are performed. For each simulation, the interaction between the spray and the wall is modelled differently. In the first simulation, the Bai-Gosman wall model [16] is used which takes different wall impingement regimes into account and provides the possibility to implement a wall film model. With this wall model, a droplet-wall interaction can end up with the droplet sticking to the wall and ending up in a liquid wall film or the droplet being reflected off the wall. However, no

FIGURE 6 Comparison simulated and experimental pressure traces.

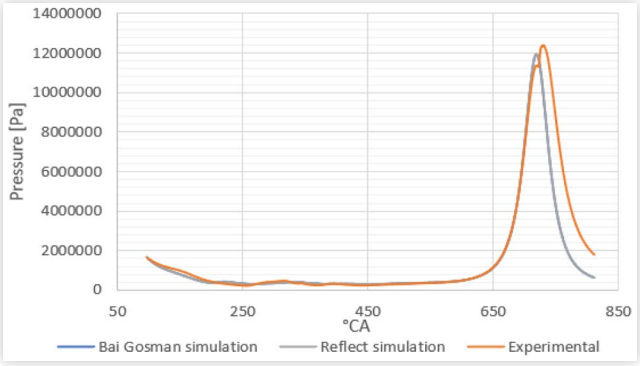

model is implemented to describe the behavior of the wall film, so droplets that end up there are practically removed from the simulation. In the second simulation, a more simplified reflect wall model is used. In this wall model, the impinging droplet can only reflect off the wall.

The validation of these models is less straight-forward compared to the validation of the NG simulation. Once again, the pressure trace is used as validation tool. Nevertheless, the pressure is also dependent on the in-cylinder trapped mass and temperature and these are dependent on the evaporation of the methanol spray. Since only few data is available about the injector properties and experimental methanol evaporation, it is difficult to exactly replicate the methanol spray and evaporation rate. Therefore, the trapped mass and temperature will differ, resulting in a difference between the simulated and experimental pressure traces.

Figure 6 shows the pressure traces for both the simulations and the experimental setup. Both the simulations show an identical pressure trace as expected, since in both simulations, 0.022g evaporated methanol ends up in the combustion chamber and temperature profiles are similar. These pressure traces overlap acceptably well with the experimental one during the main compression phase of the engine. However, as expected, towards the end of the compression stroke, the simulated pressure traces differ from the experimental pressure trace (@720 °CA). A higher peak pressure is obtained in the simulations. Since the experimental curve again takes combustion into account, and the simulation does not, this overlap in pressure should not be the case. It is expected that in the experimental setup with a methanol spray, a large amount of the injected spray will end up in a liquid wall film. Therefore, this liquid methanol can end up in the combustion chamber and evaporate there, resulting in a reduction of the in-cylinder temperature. Since this process is not captured in the simulations, this leads to a higher numerical peak pressure.

It can be concluded that the current model can capture the general engine flow behavior. However, with regards to the port-fuel injection of methanol, the current approach is not capable of accurately modeling the injection and evaporation behavior. Insights into the development of the methanol spray can be gathered from these simulations that can help improve the model in future work.

Analysis of Results

The given simulations, after validation with the experimental pressure trace, can provide some insight into the other engine operating statistics. Interesting parameters that can be obtained from a gas dynamics simulations are for example the EGR level, the turbulent intensity and flow, the mixing between air and fuel and how homogeneous this mixture is at IVC or TDC. These aspects can all help to better initialize closed cycle simulations, focused at more detailed aspects of the engine cycle, such as the combustion, at an improved numerical cost. The outcome of the gas dynamics simulations on these aspects is discussed in the next sections. Firstly, the natural gas/diesel operation is studied, after which some initial analysis on the evaporation of the methanol port fuel injection is performed.

Natural Gas/Diesel Operation

Mass Flow Figure 7 shows the mass flow through the inlet and outlet of the single-cylinder engine. A flow into the inlet duct is denoted as positive and an outward flow is denoted as negative.

From 355 °CA, a small time after the opening of the intake valve, mass starts flowing into the engine, and will thus flow into the combustion chamber. Before the closing of the intake valve at 608 °CA, it is observed that mass flows out of the engine through the inlet duct, resulting in a decrease of trapped mass in the combustion chamber. The observed oscillations before IVO and after IVC are the effect of pressure waves in the inlet duct.

In-Cylinder Mass Distribution Figure 8 shows the masses of the species present in the cylinder for the whole engine cycle. The figure confirms the observation that mass flows out of the combustion chamber again during the start of the compression stroke due to the late IVC. If the closing of the intake valve would be advanced to 558 °CA, an additional 5% in-cylinder mass could be captured.

The effective internal EGR cannot be calculated using the results from the simulation since it is not possible to take into account the air from the exhaust gas. Nevertheless, an indication of the internal EGR can be calculated using the mass of H_2O and CO_2, being 2.9% of the total mass. Furthermore, the different species concentrations can be directly retrieved from the simulations and used for the initialization of the next cycle, which is one of the major incentives for a gas dynamics simulation.

In-Cylinder Homogeneity The homogeneity in the cylinder is depicted in Figure 9. It is calculated by looking at the variation in fuel mass fraction of each computational cell inside the cylinder. When no variation is observed, thus a perfectly homogeneous air-fuel mixture is present, this is represented by a homogeneity of 1. A lower homogeneity represents a less homogeneous mixture.

The homogeneity of 1 prior to the moment mass starts flowing into the combustion chamber at 355 °CA is trivial

FIGURE 7 Inlet and outlet mass flow of the NG simulation.

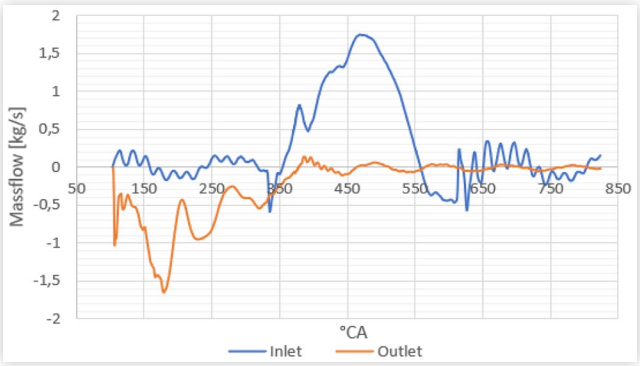

FIGURE 8 In-cylinder mass distribution of the NG simulation.

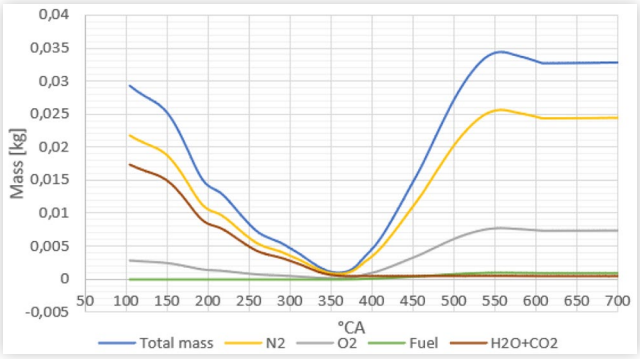

FIGURE 9 In-cylinder homogeneity NG simulation.

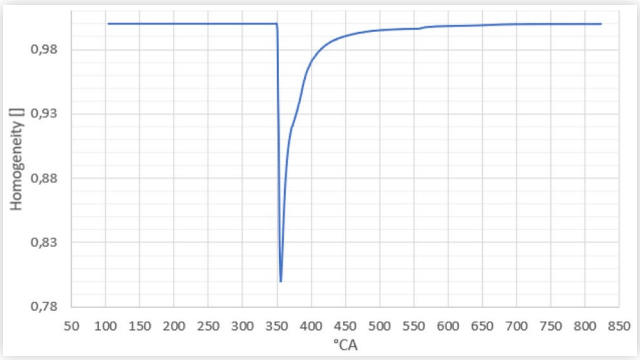

since no fuel is present in the combustion chamber yet. From 355 °CA onwards, it can be seen that due to the fuel flowing into the combustion chamber, the homogeneity will drop. Nevertheless, due to mixing of air and fuel inside the cylinder, the homogeneity will quickly increase towards 1 again. At IVC, a near perfectly homogeneous air-fuel mixture is present in the combustion chamber. It can thus be concluded that the assumption of a perfect homogeneous mixture at IVC as initialization of a combustion simulation is certainly acceptable.

Turbulent Kinetic Energy The turbulent kinetic energy represents the energy present in eddy flows generated due to turbulence. A high turbulent kinetic energy will indicate a highly turbulent flow supporting eddy currents with a lot of energy.

Figure 10 shows the total turbulent kinetic energy inside the cylinder. It can clearly be seen that the turbulent kinetic energy is generated during the intake stroke and the mass flow through the inlet valve opening. Compared to Figure 7, the turbulent kinetic energy follows the mass flow through the inlet. One can notice the correlation between the two parameters, as an increase in mass flow is accompanied by an increase in turbulent kinetic energy and vice versa. Around 700 °CA, near the end of the compression stroke, an additional small increment in the turbulent kinetic energy is observed. This is probably caused by a squish motion of the in-cylinder mass due to the geometry of the piston bowl.

Additionally, the current detailed results on in-cylinder turbulent kinetic energy, provide a means to validate more simple estimations of the TKE at IVC. For example, using these results, one can see that using the square of the mean piston speed to initialize TKE is still possible, provided a multiplier constant of 0.5 is used. This validates the assumptions mainly used for low-swirl engines, which is the case for these type of maritime engines, as shown in the next section.

Turbulence greatly influences the combustion characteristics and most of the turbulence originates from the mass flow through the intake valve opening. Therefore, the execution of a cold-flow simulation prior to a combustion simulation can be beneficial to have a better estimate of the in-cylinder turbulence.

Swirl and Tumble Motion The swirl and tumble motions are defined as the rotating motion of the mass inside the cylinder around respectively the cylinder axis and an axis orthogonal to the cylinder axis. These motions are quantified using the swirl and tumble ratio. For normal production engines, these ratios take a value between 1.0 and 2.0 [17]. Nevertheless, due to the large bore of a maritime engine, the swirl and tumble ratios are smaller.

Figure 11 shows the swirl and tumble ratio calculated from the simulation. Both the swirl and tumble ratio keep fluctuating around zero, making it difficult to quantify them. The average swirl and tumble ratio are -0.1 and -0.04 respectively. It can thus be concluded that due to the large bore of the maritime engine, no substantial swirl and tumble motions

FIGURE 10 In-cylinder turbulent kinetic energy NG simulation.

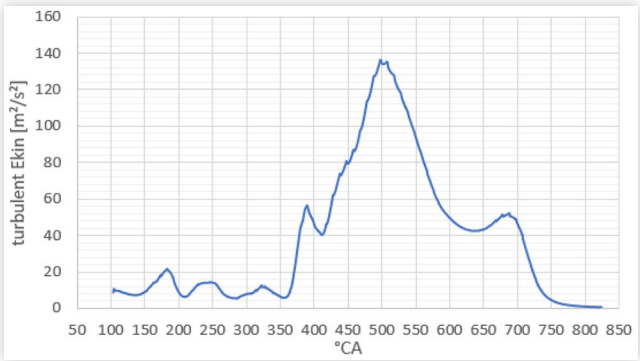

FIGURE 11 Swirl and tumble ratio NG simulation.

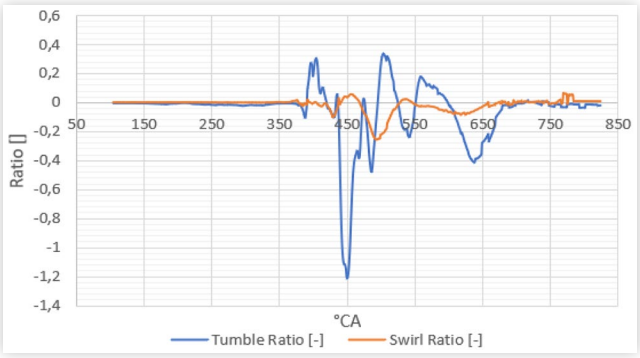

are present. Therefore, it would not be necessary to initialize these in a combustion equation.

Port Fuel Injection of Methanol

For the methanol/diesel operation one can have a more detailed look at the evaporation behavior in the intake manifold. Figure 12 shows the exchange of methanol between the Lagrangian phase (the spray) and the Eulerian phase (the mesh) when using a Bai-Gosman wall model. It shows the amount of methanol that is removed from the spray and that is added to the mesh. It can be seen that from 600 °CA onwards, these two are not the same anymore as more methanol is removed from the spray than is added to the mesh. When only concerning evaporation as the exchange of methanol between the spray and the mesh, this is not possible. Therefore, another process is taking place.

600 °CA is the moment the spray starts colliding with the walls of the inlet manifold. As already discussed, the Bai-Gosman wall model allows for the formation of a wall film. Therefore it can be concluded that the difference between the amount of methanol removed from the spray and added to the mesh is the amount of methanol that is added to a wall film as a result of the spray-wall interaction. Nevertheless, no wall film model is implemented in the simulation, thus the evaporation of the liquid wall film and the movement of the wall film in the intake manifold is not captured in the simulation. Therefore, all the methanol that is added to the wall film is in fact removed from the simulation.

Figure 13 on the other hand shows the mass exchange between the Lagrangian and Eulerian phase for the simulation with a reflect wall model. Compared with the previous simulation, it can be observed that in this simulation only evaporation is present. The methanol removed from the spray is almost equal to the methanol added to the mesh, even after 600 °CA. This simulation thus gives an idea of the effective evaporation rate of the methanol spray in the intake manifold.

The average evaporation rate after 420 °CA (when the spray is fully injected) is equal to 1.07 µg/s. This slow evaporation rate is due to the low temperature of the intake air (51°C). The actual evaporation rate in the intake manifold is assumed to be somewhat higher as derived from this simulation. This is due to the methanol in the wall film that will evaporate at a higher evaporation rate due to the hotter intake wall. Nevertheless, it can be concluded that the evaporation rate of methanol in the intake manifold is very slow.

It can thus be concluded that the Bai-Gosman model indicates that during the port fuel injection of methanol, a wall film will be formed. This wall film will aid the evaporation of methanol and therefore, a dedicated model to handle this wall film is necessary in the simulation, to better capture the experimental processes. However, based on the current results, some remarks can already be made. First, it is observed that the injected spray progresses slowly through the inlet manifold. Based on the progression of one cycle, it would approximately take three cycles for the spray to reach the intake valve. The origin of this slow progression is the combination of a large injector opening (6mm diameter) with a low mass flow rate (23.9 g/s) that result in a low injection pressure and velocity. Since a standard hollow-cone injector was used during the current experimental tests, optimizing the methanol injector to achieve a faster progression is necessary. Additionally, the spray deviates towards one intake valve, resulting in an uneven distribution of the fuel over the intake valves. Both the slow progression of the spray and uneven distribution of the fuel can be seen in Figure 14.

FIGURE 12 Comparison of the amount of fuel that is removed from spray and added to mesh with the Bai-Gosman wall model.

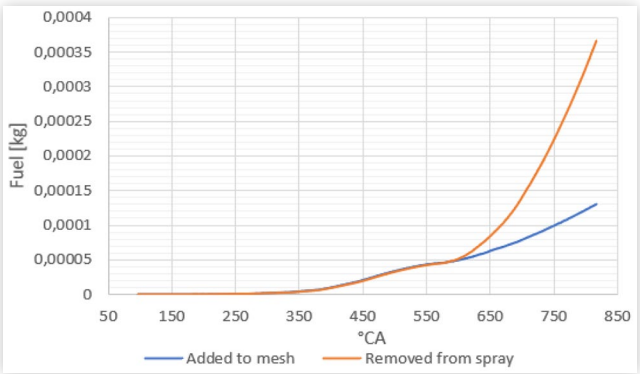

FIGURE 13 Comparison of the amount of fuel that is removed from the spray and added to the mesh with the reflect wall model

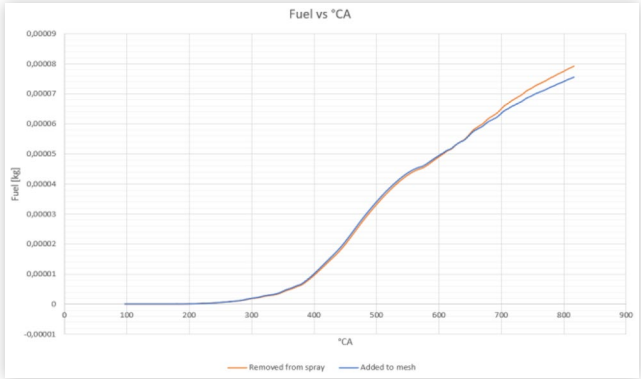

FIGURE 14 Fuel distribution [m%] and spray progression after one engine-cycle (@817 °CA).

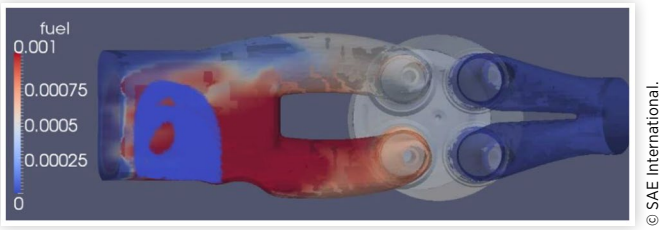

Secondly, a large portion of the injected methanol spray ends up in the wall film as was derived from Figure 12. At the end of the simulation, 0.13g methanol has evaporated and 0.24g methanol is added to the wall film. Nevertheless, as part of the spray has not yet collided with the wall, the amount of mass in the wall film is expected to be even higher. Since this wall film is an important aspect of the engine operation and can influence the behavior by for example an increased evaporation rate but also the presence of liquid pools of methanol in the cylinder, due to dripping of the intake valve, a dedicated model to handle this wall film in the simulation is necessary.

Summary/Conclusions

In this work, a cold-flow simulation was performed to investigate the internal processes of a dual-fuel marine engine with natural gas and methanol fueling conditions. The main objective of these simulations was to validate and improve the starting conditions of combustion simulations that take into account a limited engine geometry.

The simulation with natural gas fueling conditions was successfully validated against experimental data. It provided some insights to improve the initialization of a combustion equation. First, it was observed that 2.9% of the H_2O and CO_2 species were recirculated which gives an indication of the real internal EGR. The internal EGR will result in a dilution of the fresh air-fuel mixture coming into the cylinder, affecting the burning velocity during combustion. Additionally, the high specific heat capacity of the exhaust gas will take up combustion heat resulting in a drop of in-cylinder temperature and thus a decrease in NOx formation [18]. Taking the internal EGR into account in a combustion simulation will thus influence the combustion and emission behavior.

Secondly, it was confirmed that a uniform distribution of the species inside the combustion chamber can be used as starting condition for a combustion simulation. Furthermore, it also appeared that almost no swirl and tumble motion is present in the combustion chamber. This was expected as a marine engine is not designed to attain large swirl and drag motions due to its larger bore diameter.

Lastly, it was observed that the main origin of turbulence in the combustion chamber is the intake flow along the intake valves. During combustion, the turbulence will result in wrinkling of the flame front, increasing the effective flame surface area which will speed up the mass burning rate [18]. Especially in NG dual-fuel engines where problems with combustion at part load are retrieved, an exact estimation of the turbulence coming from the intake valve can be of great importance.

The simulation with methanol fueling conditions could not be completed as the model was not able to capture the exact evolution of the methanol spray. However, it provided some insights that could be valuable for further research. First, it was concluded that the methanol spray showed a very slow progression through the intake manifold. It could take up to 3 cycles before the spray would reach the intake valve. This slow progression was assumed to be due to the combination of a large nozzle opening with a low mass flow rate that resulted in a low injection pressure and velocity. An optimized methanol injector could tackle these issues.

Secondly, due to the low temperature in the intake manifold, a low average evaporation rate in the intake manifold of only 1.07 µg/s was observed. It could therefore be necessary to bypass the intercooler, after the turbocharger, to obtain more favorable evaporation rates. The evaporation of methanol itself could then provide the necessary cooling for the air-fuel charge.

Lastly, it was observed that the bulk of the injected methanol spray would end up in a liquid wall film. Therefore, since no wall film model is present in the model, it was not possible to extract the exact locations where most evaporation would occur. Nevertheless, these locations are most likely in the wall film near the hot wall/intake valve or in the combustion chamber as liquid methanol could drip from the wall film through the intake valves. A dedicated wall film model is therefore necessary to study these effects and capture their influence on the engine behavior.

It can be concluded finally that the execution of a cold-flow simulation prior to a combustion simulation provides valuable insights to improve the initialization of the combustion simulation and attain a more realistic combustion behavior. In future work therefore, the effect of the currently observed trends will be investigated during closed cycle dual-fuel combustion simulations, in order to achieve a proper prediction of the behavior of such an engine.

References

1. COM(2015) 81 final/2, "The Paris Protocol - A Blueprint for Tackling Global Climate Change Beyond 2020," 2015, European Commission, Brussels.
2. Dieselnet, "IMO Marine Engine Regulations," 2018, https://www.dieselnet.com/standards/inter/imo.php
3. Dierickx, J., Beyen, J., Block, R., Hamrouni, M. et al., "Strategies for Introducing Methanol as an Alternative Fuel for Shipping," in *7th Transport Research Arena TRA 2018 (TRA 2018)*, 2018, Ghent University.
4. Cantore, G., Mattarelli, E., Rinaldini, C.A., Savioli, T. et al., "Numerical Optimization of the Injection Strategy on a Light Duty Diesel Engine Operating in Dual Fuel (CNG/Diesel) Mode," 2019.
5. Singh, S., Krishnan, S.R., Srinivasan, K.K., Midkiff, K.C. et al., "Effect of Pilot Injection Timing, Pilot Quantity and Intake Charge Conditions on Performance and Emissions

for an Advanced Low-Pilot-Ignited Natural Gas Engine," *International Journal of Engine Research* 5(4):329-348, 2004.

6. You, J., Liu, Z., Wang, Z., Wang, D. et al., "Impact of Natural Gas Injection Strategies on Combustion and Emissions of a Dual Fuel Natural Gas Engine Ignited with Diesel at Low Loads," *Fuel* 260:116414, 2020.
7. Wei, L., and Geng, P., "A Review on Natural Gas/Diesel Dual Fuel Combustion, Emissions and Performance," *Fuel Processing Technology* 142:264-278, 2016.
8. Imran, S., Emberson, D.R., Diez, A., Wen, D.S. et al., "Natural Gas Fueled Compression Ignition Engine Performance and Emissions Maps with Diesel and RME Pilot Fuels," *Applied Energy* 124:354-365, 2014.
9. Maghbouli, A., Saray, R.K., Shafee, S., and Ghafouri, J., "Numerical Study of Combustion and Emission Characteristics of Dual-Fuel Engines Using 3D-CFD Models Coupled with Chemical Kinetics," *Fuel* 106:98-105, 2013.
10. Mousavi, S.M., Saray, R.K., Poorghasemi, K., and Maghbouli, A., "A Numerical Investigation on Combustion and Emission Characteristics of a Dual Fuel Engine at Part Load Condition," *Fuel* 166:309-319, 2016.
11. Methanol Institute, "Methanol Production, 2020, https://www.methanol.org/methanol-production/, accessed May 22, 2020.
12. Soni, D.K. and Gupta, R., "Optimization of Methanol Powered Diesel Engine: A CFD Approach," *Applied Thermal Engineering* 106:390-398, 2016.
13. Verhelst, S., Turner, J.W., Sileghem, L., and Vancoillie, J., "Methanol as a Fuel for Internal Combustion Engines," *Progress in Energy and Combustion Science* 70:43-88, 2019.
14. Dierickx, J., Sileghem, L., and Verhelst, S., "Efficiency and Emissions of a High-Speed Marine Diesel Engine Converted to Dual-Fuel Operation with Methanol," in *CIMAC World Congress on Combustion Engine*, 2019, 1-14, CIMAC.
15. Coulier, J. and Verhelst, S., "Using Alcohol Fuels in Dual Fuel Operation of Compression Ignition Engines: A Review," in *28th CIMAC World Congress on Combustion Engine*, 2016, 1-12, CIMAC.
16. Bai, C. and Gosman, A., "Development of Methodology for Spray Impingement Simulation," *SAE Transactions* 104:550-568, 1995.
17. Lumley, J.L., *Engines: An Introduction* (Cambridge University Press, 1999).
18. Verhelst, S., "Volumetric Pumps, Compressors and ICE Fundamentals," Syllabus. Ghent University, Faculty of Engineering and Architecture, 2018.

Contact Information

Gilles Decan
Department of Electromechanical,
Systems & Metal Engineering,
Ghent University
Sint-Pietersnieuwstraat 41
B-9000 Ghent, Belgium
gilles.decan@ugent.be

Acknowledgments

This research has been funded by Ghent University (Belgium) through GOA project [BOF16/GOA/004]. The authors gratefully acknowledge the financial support. The authors also want to express their sincere appreciation to the Anglo Belgian Corporation, a manufacturer of medium speed engines, and WTZ Roßlau for the experimental data they provided.

Definitions/Abbreviations

ABDC - After Bottom Dead Center
AFR - Air-Fuel Ratio
ATDC - After Top Dead Center
BBDC - Before Bottom Dead Center
BTDC - Before Top Dead Center
CA - Crank Angle
CFD - Computational Fluid Dynamics
DSR - Diesel Substitution Ratio
EGR - Exhaust Gas Recirculation
EVC - Exhaust Valve Closing
EVO - Exhaust Valve Opening
ICE - Internal Combustion engine
IVC - Inlet Valve Closing
IVO - Inlet Valve Opening
LHV - Lower Heating Value
LBV - Laminar Burning Velocity

ISSN 0148-7191